Energy & Environmental Science

PERSPECTIVE

Oxygen diffusion in solid oxide fuel cell cathode and electrolyte materials: mechanistic insights from atomistic simulations

Alexander Chroneos,*[ab] Bilge Yildiz,*[c] Albert Tarancón,*[d] David Parfitt[a] and John A. Kilner*[a]

Solid oxide fuel cells are of technological interest as they offer high efficiency for energy conversion in a clean way. Understanding fundamental aspects of oxygen self-diffusion in solid state ionic systems is important for the discovery of next-generation electrolyte and cathode material compositions and microstructures that can enable the operation of SOFCs at lower temperatures more efficiently, durably, and economically. In the present perspective article, we illustrate the important role of modelling and simulations in providing direct atomic scale insights on the oxygen ion transport mechanisms and conduction properties in the cathode and electrolyte materials, and in accelerating the progress from *old* materials to *new* concepts. We first summarize the ionic transport mechanisms in the traditional cathode and electrolyte materials which have been widely studied. We then pay our attention to the non-traditional materials and their oxygen transport paths from recent studies, focusing on structural and transport *anisotropy* and *lattice dynamics*. Lastly, we highlight the new developments in the potential to increase the ionic conductivity of the traditional materials through external mechanical stimuli, bringing about the *mechano-chemical* coupling to drive fast ionic transport.

1. Introduction

The interest in Solid Oxide Fuel Cell (SOFC) technology is driven by their potential for high efficiency energy conversion with reduced emission of green house gases compared to other more conventional power generation routes.[1,2] At the present high operating temperatures (up to 1000 °C), SOFCs operate with hydrogen as well as existing fossil fuels and efficiently convert chemical energy to electricity, and *vice versa*. They are also used in combined heat and power applications.[3–5] These high operating temperatures, however, lead to high costs mainly due to materials challenges in thermal cycling, chemical and microstructure degradation, and expensive constituents in interconnects and heat exchangers.[3] A way to address these challenges is by lowering the operating temperatures of SOFCs to the intermediate temperature range (500–700 °C). The reduction in temperature is, on the other hand, accompanied by an increase in the losses for reaction and transport kinetics in all layers of the cell. Of particular concern are the cathode and electrolyte which have major contributions to the inefficiencies at low temperatures. There is thus a need to search for new classes of materials that can maintain high rates of oxygen transport even at reduced temperatures.

[a]Department of Materials, Imperial College London, London, SW7 2AZ, UK. E-mail: alexander.chroneos@imperial.ac.uk; j.kilner@imperial.ac.uk
[b]Department of Materials Science and Metallurgy, University of Cambridge, Cambridge, CB2 3QZ, UK
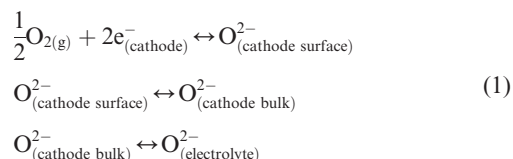*[c]Laboratory for Electrochemical Interfaces, Department of Nuclear Science and Engineering, Massachusetts Institute of Technology, 77 Massachusetts Avenue, Cambridge, MA, 02139, USA. E-mail: byildiz@mit.edu*
[d]Department of Advanced Materials for Energy, Catalonia Institute for Energy Research (IREC), C/Jardí de les Dones de Negre, Planta 2, E-08930 Sant Adrià del Besòs, Spain. E-mail: atarancon@irec.cat

Broader context

Advances in the field of solid state ionics for energy conversion are necessary to address the challenge of attaining cleaner and sustainable sources of energy. In this framework high temperature electrochemical devices based on ceramic oxide materials have a crucial role to play in decarbonising the future energy mix. Current targets of cost and durability necessitate solid oxide fuel cells to operate in the intermediate temperature range (500–700 °C). To achieve these targets oxygen diffusion in both the cathode and the electrolyte of the solid oxide fuel cell needs to be enhanced. This feature article illustrates the role of atomic scale modelling in providing fundamental insights into the oxygen migration mechanism and how it is affected by the structure, oxygen stoichiometry, and lattice strain.

The key to enable such intermediate temperature range of operation is to accelerate the oxygen reduction reaction in the cathode and the oxygen transport in the cathode and electrolyte. At a high level, the overall reactions involving oxygen are:

$$\frac{1}{2}O_{2(g)} + 2e^-_{(cathode)} \leftrightarrow O^{2-}_{(cathode\ surface)}$$

$$O^{2-}_{(cathode\ surface)} \leftrightarrow O^{2-}_{(cathode\ bulk)} \qquad (1)$$

$$O^{2-}_{(cathode\ bulk)} \leftrightarrow O^{2-}_{(electrolyte)}$$

The first reaction stands for the reduction of oxygen on the cathode surface, the second reaction represent diffusion of oxygen into the cathode, and the third reaction represents transfer of oxygen from the cathode to the electrolyte in which the oxygen ion proceeds to diffuse. As one or more of the reactions involved in eqn (1) have high activation energies, a reduction of the operating temperature leads to significant electrical energy losses. Traditional cathodes such as $La_{1-x}Sr_xMnO_{3-\delta}$, which are good electronic conductors are no longer appropriate alone due to their poor bulk ionic conductivity, whereas mixed ionic-electronic conductors (MIEC) have been considered a viable solution.[6] Adler *et al.*[7,8] demonstrated that the oxygen reduction reaction in MIEC electrodes is governed by the oxygen surface exchange and the oxygen diffusion.

Electrolytes for SOFCs also should exhibit high ionic conductivity, however, combined with low electronic conductivity. Other requirements for the electrolyte of SOFCs are stability under both oxidation and reduction conditions, long term chemical stability and mechanical compatibility with the electrode materials.[3]

The oxygen transport properties at the cathode and electrolyte materials are not only of technological interest as noted above, but also of fundamental importance.[9–20] The energetics of oxygen transport in these oxides are affected by the material structure, composition, oxygen stoichiometry, doping and elastic strain, which comprise a wide range of parameter space in optimizing the transport properties. In combination with validation and verification experiments, predictive computational materials approaches provide a rational and efficient materials design route for fast oxygen ion conduction in SOFC materials. Especially the simulations at the electronic and atomic scale offer the opportunity to gain detailed insight for the formation and transport of charged defects in a wide variety of inorganic materials,[21–27] and thus, the capacity to control their properties.

In this perspective article, we focus on the oxygen diffusion mechanisms and energy barriers of a subset of contemporary cathode and electrolyte materials; pushing the topic from old materials to new concepts. The experimentally demonstrated conductivities of the new concepts in comparison to the traditional electrolyte and electrode materials are shown in Fig. 1. The superior transport in these new materials/structures, and the capability to identify the governing transport mechanisms in them make the basis for the motivation of this perspective article. The emphasis is on recent mechanistic insights from computational modelling at the electronic- and atomistic scales. A common theme among the new materials reviewed here is the anisotropy of the structure and/or the preferred migration path, and the role of the flexibility and dynamics of polyhedral structures surrounding the ion conduction path. Whenever possible the predictions are discussed in view of experimental investigations.

The article is structured as follows. First, we briefly describe the application of these materials, diffusion mechanisms and the relevant computational methodologies. Thereafter, we discuss in detail the cathode materials emphasizing the recent molecular dynamics (MD) studies, focusing on the layered and anisotropic classes of materials; Ruddlesden-Popper series and double perovskites such as $GdBaCo_2O_{5+\delta}$ which have recently become of high interest.[9–20] This is followed by the discussion of the electrolyte materials and structures, ranging from a brief overview of the traditional cubic-like-symmetry isotropic systems, the

Alexander Chroneos

Dr Alexander Chroneos gained his MSc in Theoretical Chemistry from the University of Oxford and his PhD from Imperial College London (2008). He has worked as a research associate at the University of Münster (2008), Imperial College London (2008–2010) and Cambridge University (2010–2011). Alexander has been involved in research in a range of areas of materials science and applied physics focusing on materials for microelectronic and energy applications including nuclear, photovoltaic and solid oxide fuel cell materials. He has published over 70 scientific papers and 2 invited chapters on these and related topics. He is presently a Marie Curie Fellow at the Institute of Materials of NCSR Demokritos.

Albert Tarancón

Dr Albert Tarancón is a Senior Scientist and Head of the Nanoionics and Fuel Cells Group of the Advanced Materials for Energy Department at the Catalonia Institute for Energy Research (IREC). His research interest is primarily concerned with materials for alternative energy technologies and their applicability in powering portable devices. He is deeply involved in the electrical characterization of materials for intermediate temperature solid oxide fuel cells, solid oxide electrolyzers and thermoelectric generators. A particular field of interest is the integration of nanoionics concepts in micro-Solid Oxide Fuel Cells.
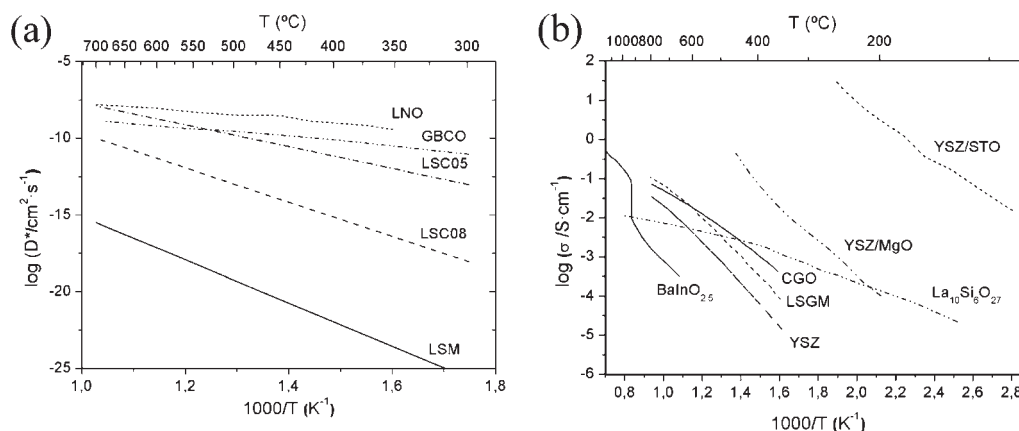
Fig. 1 Arrhenius plots of (a) measured oxygen tracer diffusivity for different oxide cathodes: $La_{0.8}Sr_{0.2}MnO_{3-\delta}$ (LSM, ref. 29), $La_{0.5}Sr_{0.5}CoO_{3-\delta}$ (LSC05, ref. 29), $La_{0.8}Sr_{0.2}CoO_{3-\delta}$ (LSC08, ref. 29), $GaBaCo_2O_{5+\delta}$ (GBCO, ref. 17), $La_2Ni_2O_{4+\delta}$ (LNO, ref. 30), and (b) measured oxide ionic conductivity for different oxide electrolytes: $ZrO_2:Y_2O_3$ (YSZ, ref. 31), $CeO_2:Gd_2O_3$ (CGO, ref. 31), $La_{0.9}Sr_{0.1}Ga_{0.9}Mg_{0.1}O_{3-\delta}$ (LSGM, ref. 32), $BaInO_{2.5}$ (ref. 33), $La_{10}Si_6O_{27}$ (ref. 34), strained YSZ over single crystals of MgO (ref. 35) or between single crystal layers of $SrTiO_3$ (ref. 36). We note that the conductivity reported for the YSZ/STO system (ref. 36) has not been conclusively confirmed or disproved to be fully ionic conductivity at this time.

yttria-stabilized zirconia (YSZ) and $La_{1-x}Sr_xGa_{1-y}Mg_yO_3$ (LSGM), to the non-cubic systems as the Brownmillerites and Apatites where the effect of anisotropy and lattice dynamics are highlighted, and lastly back to the traditional systems where the effect of lattice strain is highlighted in potentially accelerating the oxygen transport kinetics. Finally, we conclude and present an outlook for the future in search for new classes of cathode and electrolyte materials for SOFCs. This feature article is not a comprehensive review of all possible cathode and electrolyte materials. There are other relevant comprehensive reviews of related materials covering a wider spectrum of properties of technological and fundamental importance.[28–46] The references and discussions herein are selected to guide the readers towards

the direct atomistic insights gained from simulations in this context. The capability to assess the ionic transport mechanisms and energetics directly from the electronic- and atomic-scale description of such oxide ion systems is of both scientific and industrial importance in discovering new compositions and structures for SOFCs.

2. Applications

High temperature electrochemical devices based on solid oxide materials have a vital role to play in decarbonising the future energy mix. This ranges from their use in SOFCs, Solid Oxide Electrolysis Cells (SOECs) and in clean energy related processes such as oxygen separation membranes for Carbon Capture and

Prof. Bilge Yildiz received her PhD in 2003 in Nuclear Science and Engineering at Massachusetts Institute of Technology (MIT) in the US, and her BSc in 1999 in Hacettepe University in Turkey. After working as a postdoctoral researcher at MIT and research staff at Argonne National Laboratory on electrochemical devices and materials for hydrogen fuel- and electrolytic-cells, she came back to MIT as an assistant professor in 2007. Her research focuses on probing the transport and reac-

Bilge Yildiz

tivity mechanisms at interfaces and surfaces of solid state ionic materials driven by harsh environments, by integrating computational and surface sensitive in situ experimental techniques. Major applications in her research program include solid state ionic materials of importance to solid oxide fuel- and electrolysis-cells and to surface passive films in metallic corrosion.

John A. Kilner

Prof. John Kilner gained his PhD from Birmingham University and joined Imperial College in 1979. In 1995 he was appointed Professor of Materials Science and in 2006, BCH Steele Professor of Energy Materials.

John has over 30 years experience in the measurement of mass transport in ceramic materials for Solid Oxide Fuel Cells (SOFCs) and Ceramic Oxygen Generators (COGs). He has published over 300 scientific papers. He is currently the European editor of Solid State Ionics and is the holder of numerous patents. He is a co-founder of the AIM listed company Ceres Power Ltd, winner of the European Fuel Cell Forum Schönbein gold medal, the Verulam medal of the IOMMM, and the recipient of the 2005 Royal Society Armourers and Braziers award.

Storage (CCS) systems. In all the three applications mentioned above key components of the devices are the mixed conducting oxide materials, the cathode for the SOFC, the anode for the SOEC and the active membrane in the oxygen separator. For example it is well established that for the SOFC to meet current targets of cost and durability, operation in the intermediate temperature range (500–700 °C) is a particularly attractive development. It is also well established that in this temperature range (and below) the cathode provides the greatest source of losses, followed by the electrolyte, due to the high polarisation resistances found for most materials in current use. It is thus of paramount practical importance to gain insights into the mechanisms of migration of oxygen in a range of structures and compositions, and in particular to identify any trends that might occur, to optimise oxygen transport (for example by modifying the oxygen stoichiometry, composition and cation disorder) in mixed conductors and ionic conductors for SOFC cathode, electrolyte and other related applications. This problem is a good example of where simulations, either atomistic or first principles-based, can be of enormous benefit in identifying such trends.

3. Diffusion mechanisms

Diffusion in oxide materials is a fundamental and physically complex phenomenon. The difference from metals is that the existence of the anion and cation sublattices restricts ionic diffusion to its own sublattice,[47–49] while it is still influenced by the behaviour of the cation sublattice. In oxides it is common to consider the anion and cation sublattices separately. In most technologically interesting oxide materials oxygen self-diffusion is significantly faster than cation diffusion.[50]

Diffusion in crystalline materials requires the migration of atoms away from their equilibrium positions. Diffusion mechanisms describe the way an atom can move from one equilibrium position to the neighbouring one. The role of point defects in enabling this motion is critical.[47] For the oxide materials considered here, there are three generally accepted mechanisms, and all three depend on the nature of the point defects in the system: the interstitial, the interstitialcy and the vacancy mechanisms. In the specific examples for cathodes and electrolytes presented in this paper, we will also highlight other mechanisms, which are initiated by the presence of point defects but in addition involve cooperative motion of the local polyhedral structures.

In the interstitial mechanism, ions positioned at interstitial sites in the lattice migrate by jumping from one interstitial site to a neighbouring interstitial site. When a single jump is completed there is no permanent displacement of the other ions. The interstitial mechanism does not require the existence of other defects except from the interstitial ions themselves. The interstitialcy mechanism is different from the direct interstitial mechanism, as an interstitial ion displaces an ion from its equilibrium lattice site.[20] Thereafter the displaced ion moves to another interstitial site.

In the vacancy mechanism of diffusion, a host ion diffuses by jumping to a neighbouring vacancy.[31] The vacancy mechanism commonly governs oxygen transport, prevalent for oxygen self-diffusion in a number of hypostoichiometric fluorite- and perovskite-related systems[28] traditionally of interest to SOFC. In the vacancy mechanism the presence of lattice vacancies is necessary, and their concentration in the lattice will influence the kinetics. The energy barriers for this mechanism are typically high limiting the applicability of these materials for SOFC applications to temperatures over 900 K, *i.e.* at temperatures where $\sigma > 0.01$ S cm^{-1} for self-supported electrolytes.[2] For example, a reduction of temperature from 900 °C to 500 °C (1173 K to 773 K) reduces the oxygen ion conductivity by two orders of magnitude in 10% yttria doped ZrO_2.[2] The migration paths of an oxygen anion in the cubic symmetry systems most common to SOFC materials are shown in Fig. 2, representing the fluorite structure adopted by doped ZrO_2 and CeO_2 as conventional electrolyte materials in (a) and (b), and the perovskite structure adopted by $LaGaO_3$ as a conventional electrolyte material,[41] and by $LaMnO_3$ and $LaCoO_3$ as conventional cathode materials in (c) and (d).

The migration enthalpies, or energy barriers, for the thermally activated oxygen ion hopping through these paths are the critical descriptor for how low a temperature the electrolyte and cathode can effectively function at. In the transition state theory framework,[52] the oxygen ion exchange rate with vacancies, v, along the migration paths is represented by the Boltzmann relationship as,

$$v = v_0 \exp\left(\frac{-E_M}{k_B T}\right) \qquad (2)$$

where E_m denotes the migration barrier along this path and v_o is a constant. The vacancy diffusivity, D_v, is related to the mean square displacement $\langle R^2 \rangle$ of the oxygen vacancies through the Einstein relation,

$$\langle R^2 \rangle = 6D_v t. \qquad (3)$$

D_v exponentially depends on the energy barrier for oxygen vacancy migration, E_B, similar to the formalism in eqn (2). The oxygen diffusivity D_O is related to the D_v considering the balance between the fluxes of oxygen atoms and vacancies as,

$$D_O = \frac{c_v}{1 - c_v} D_V \qquad (4)$$

where c_v is the vacancy concentration fraction. Note that at small values of c_v, D_0 scales almost linearly with c_v. On the other hand, a change in the migration barrier, E_B, affects D_v and D_0 *exponentially*, making this factor an important target to reduce for the intermediate temperature functionality of SOFC materials.

The oxygen migration energy depends on the following key factors in the material in the vicinity of the migration path:[38,53–56] (1) the cations surrounding the oxygen path, in particular the bridging cation pair through which the oxygen passes, (2) the distance and configuration of the vacancies near the initial and final site of the vacancy, and (3) the distance and configuration of the dopant cations near the initial and final site of the vacancy. All three factors influence the system's potential energy landscape and the corresponding migration barriers. These defect–defect interactions, analyzed in detail by Bogicevic et al.[37] and summarized recently by Kushima and Yildiz[38] for the YSZ system, are related to the association (binding) energies of the vacancy–vacancy, dopant–dopant, and vacancy–dopant clusters, and are governed by the electrostatic, electronic, and elastic parts. Among these three types of defect–defect interactions, the
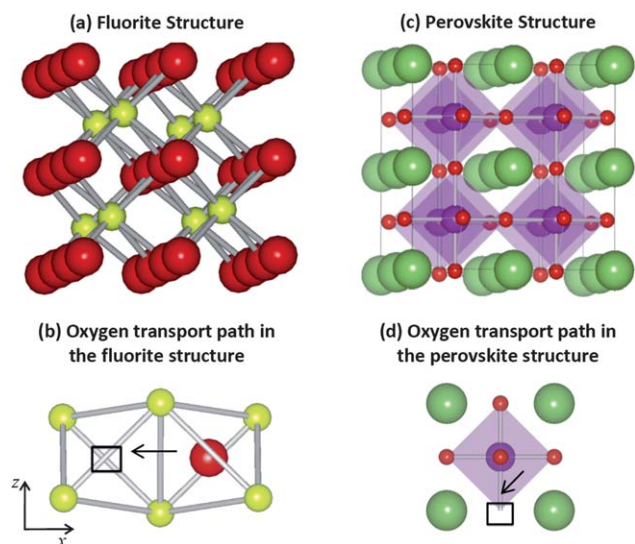
Fig. 2 Crystal structure and oxygen migration path in the fluorite structure (a, b), representative of ZrO_2 and CeO_2 systems (red/large, and yellow/small spheres are oxygen and cation sites, square is vacant oxygen site), and in the perovskite structure (c, d), representing $LaGaO_3$, $LaMnO_3$ and $LaCoO_3$ systems (red/small, green/large, and purple/medium spheres are oxygen, A-site cation, and B-site cation sites, square is vacant oxygen site). Arrows in (b) and (d) show schematically the path for the oxygen migration towards the vacant site.

vacancy–vacancy interaction is the strongest followed by the vacancy–cation interaction, and the cation–cation interaction is the weakest of the three.[37] Vacancy–cation interactions, in part, determine the relative position of the vacancy with respect to the host and the dopant cations; for example vacancies in equilibrium reside as first nearest neighbour (NN) to the Zr and second NN to the Y (a large cation) in 8% yttria doped ZrO_2 due to elastic relaxations.[39] The vacancy–vacancy and cation–cation interactions primarily determine the clustering or ordering tendency of these defects. For example, vacancies locate themselves randomly maximizing the distance among themselves on the basis of dominant electrostatic interactions in up to 10% yttria doped YSZ.[57] The dopant cation pairs, Y–Y, as first NN are found slightly more favourable than the second NN Y–Y pairs in YSZ.[37,58] Recent theoretical results by Predith *et al.*[24] show that long range ordering of the dopant cations exists in YSZ at high dopant concentrations, this cation ordering could exist in short range at the lower yttria concentration range, and such short-range order of yttrium cations may be responsible for the observed decline in ionic conductivity beyond the 8% yttria doping level in YSZ. To minimize energy barrier along the migration path, the electrostatic, electronic, and elastic interactions should balance in the vicinity of the migration path so that there is neither a very strong association nor a very strong repulsion at the initial and final state of the oxygen vacancy.[24] Therefore, the limits of ionic conductivity in the context of vacancy mediated transport in these cubic symmetry systems depend directly on the bond strength between the oxygen and the neighbouring cations, which is influenced by the local defect–defect interactions.

The ultimate stable configuration of dopants and vacancies is governed by the thermodynamics of the structure. On the other hand, one could identify procedures to fix a special distribution of dopants in order to minimize the energy barriers or modify the nature of the oxygen migration for increasing the oxygen diffusivities beyond the currently reported values in these materials. However, to engineer and keep these *ad hoc* dopant distributions under conditions of relevance to SOFCs may be a daunting job. In the meantime, the search for alternative oxide ion conducting cathode and electrolytes with equilibrium structures and compositions continues.

4. Computational methods

In this article, most of the discussion and results taken from literature is based on atomistic scale MD and density functional theory (DFT) frameworks. Therefore we will summarize key points on these methods in what follows. For further details regarding atomic scale modelling as applied to inorganic solids the reader is referred to comprehensive relevant reviews.[59–61]

In solid state physics the quantum mechanical formulation provides the most complete description of nature. However, even though there are analytic solutions of the Schrödinger equation for some simple systems (*e.g.* hydrogen atom) solving the equation for a large number of electrons is computationally intensive and currently insurmountable computationally because of the complexity of many-electron interactions.[62] To overcome these issues and constitute the simulation of solids tractable, suitable approximation techniques such as DFT have been developed.[63,64] Commonly for oxides, in DFT the exchange-correlation energy is described in the local density approximation (LDA) or the generalized gradient approximation (GGA). Another way of approximating the exchange-correlation energy is with the use of hybrid functionals that incorporate a part of the exact exchange from the Hartree–Fock theory.[65] Generally, a plane-wave basis set is used with the pseudopotential method. In this, the core electrons are described by effective potentials (pseudopotentials) and the valence electrons may evolve explicitly. Important recent developments include the introduction of the U-parameter (on-site Coulomb interaction parameter) for open-shell transition metal compounds. Within the DFT framework the activation energy of diffusion can be calculated coupled with techniques to identify the minimum energy path, such as the nudged elastic band method.[66] The limitation of DFT is the relatively small simulation size that is typically on the order of only a few hundred atoms at the present time. While this size is suitable for bulk, and to some extent the surface properties, it does not allow the treatment of extended defects and microstructures without introducing artefacts of defect–defect interactions among the neighbouring simulation cells.

The classical potential-based MD method is another widely used technique to study diffusion in oxides. In MD the state of the system is described in terms of the positions and the momenta of all the particles that constitute it. Newton's equations of motion for an ensemble of particles are solved iteratively. These particles interact *via* potential energy functions, within the classical Born-like description of the ionic crystal lattice.[67] Ionic interactions are described by a long-range Coulombic term and by a short-range parameterized pair potential such as the Buckingham potential.[68–70] In MD simulation systems that are orders of magnitude higher compared to DFT can be simulated.

On the other hand, issues in accuracy can arise especially when the description of the electronic structure of the system becomes important (*i.e.* charge transfer phenomena on surfaces), and treatment of structures that deviate from the bulk as on surfaces and at interfaces.

5. Oxygen transport mechanisms in cathodes

Numerous mixed ionic and electronic oxides are presently being considered and investigated for SOFC cathode applications. A number of perovskite structured materials with general formula $La_{1−x}Sr_xMO_{3−d}$ (M = Mn, Fe, Co) are among the most traditionally and widely studied cathode materials.[71] These possess a cubic-like symmetry with oxide ion diffusion based on the vacancy migration mechanism, as illustrated in Fig. 2. In the present feature article, instead of these traditional cathodes[72] and the oxygen reduction and transport in them, we focus in detail the progress in oxygen transport in perovskite-related phases with anisotropic structures and with oxide ion transport that does not rely only on oxygen vacancies; Ruddlesden Popper (RP) series of layered oxides (formula $A_{n+1}B_nO_{3n+1}$); the double perovskites (formula $AA′B_2O_{5+\delta}$); and layered cobaltites and ferrites exemplified by $Sr_{1−x}Y_xCoO_{3−\delta}$ and $Sr_4Fe_6O_{13}$, respectively.

5.1. Ruddlesden-Popper series of layered oxides

Here we will concentrate on the first members of the RP series (for $n = 1$, A_2BO_4) such as $La_2NiO_{4+\delta}$, $La_2CoO_{4+\delta}$ and $Pr_2NiO_{4+\delta}$. These have the K_2NiF_4 structure which has been investigated in great detail ever since the observation of high-temperature superconductivity in $La_{2−x}Ba_xCuO_4$.[73] It was determined with the use of *in situ* high temperature neutron powder diffraction that La_2NiO_4 exhibits the tetragonal symmetry (space group $I4/mmm$) in the temperature range 423–1073 K.[74]

The polymorphs of K_2NiF_4 are dependent upon the temperature and changes in stoichiometry. Interestingly, these materials, especially if doped, can be both hypostoichiometric (*i.e.* oxygen deficient) and hyperstoichiometric (*i.e.* oxygen excess). In hypostoichiometric materials there exist oxygen vacancies (represented by $V_O^{\cdot\cdot}$ in Kröger–Vink notation), whereas in hyperstoichiometric oxygen interstitials (represented by O_i'' in Kröger–Vink notation). These point defects are important for the oxygen diffusion, and the defect–defect interactions are significant in the RP layered compounds; this is both a result of Coulomb repulsion between oxygen interstitials and the interaction of elastic strain fields surrounding the defects. The oxygen diffusion coefficient D_O can be defined as:

$$D_O = D_V[V_O^{\cdot\cdot}] + D_i[O_i''] \qquad (5)$$

where D_V and D_i are the vacancy and interstitial diffusion coefficients, $[V_O^{\cdot\cdot}]$ and $[O_i'']$ are the oxygen vacancy and interstitial site fractions, respectively.

For example, in hypostoichiometric $La_{2−x}Sr_xCuO_{4−\delta}$ Opila *et al.*[75] determined that there is significant anisotropy between the oxygen diffusion in the *a–b* plane and the *c*-axis. In tetragonal $La_{1.85}Sr_{0.15}CuO_{4−\delta}$ the MD investigations of Savvin *et al.*,[76] revealed oxygen diffusivities that were higher by several orders of magnitude compared to previous stable isotope diffusion

studies on dense polycrystalline samples.[77] Nevertheless, for $La_{1.85}Sr_{0.15}CuO_{4−\delta}$ the MD activation energy of diffusion of (0.86 eV)[76] is in excellent agreement with the determined value (0.84 eV).[77]

Conversely, previous thermogravimetric analyses of $La_2NiO_{4+\delta}$ have revealed a range of oxygen hyperstoichiometries that are dependent upon the experimental conditions.[14,78] Recent MD simulations predicted that the oxygen ion diffusivity in the RP materials $La_2NiO_{4+\delta}$, $Pr_2NiO_{4+\delta}$ and $La_2CoO_{4+\delta}$ occurs *via* a highly anisotropic interstitialcy mechanism with almost all of the migration taking place in the *a–b* planes (refer to Fig. 3).[30,79–81] The experimental values for the activation energy of migration are within the range of values predicted from the MD calculations (refer to Table 1). For $Pr_2NiO_{4+\delta}$ oxygen diffusivities were calculated for a range of hyperstoichiometries and there is excellent agreement between the absolute calculated values and those observed experimentally.[14,80] However, the calculated values for the activation energy of migration depend strongly upon the degree of hyperstoichiometry [range from 0.49 eV ($\delta = 0.025$) to higher values 0.64 eV ($\delta = 0.20$)].[80] The dependence of the oxygen diffusion coefficient on the concentration of interstitials (or degree of hyperstoichiometry) also contains useful mechanistic information. In a similar way as described above for vacancies, the oxygen interstitial diffusivity, D, at a temperature T is formulated as,[80]

$$D = D_i[O_i] \exp(−E_m/k_BT) \qquad (6)$$

where $[O_i]$ is the concentration of oxygen interstitials, D_i is the pre-factor term, E_m is the energy barrier to migration and k_B is Boltzmann's constant.[73] Initially the diffusivity rises rapidly as we increase the concentration of oxygen interstitials. This is expected as the interstitials mediate the oxygen diffusion process. Notably, beyond $\delta \approx 0.02$ the diffusivity levels off (refer to Fig. 4). The physical meaning of this process can be attributed to the rise in the effective migration barrier due to the increased formation energy of oxygen interstitials (due to the presence of other pre-existing neighbouring interstitials) and the stiffening of the lattice. The latter is due to the pinning of the NiO_6 sub-lattice because of the additional oxygen interstitials (see Fig. 3), which in turn reduces the ease with which the octahedra tilt to allow the passage of the migrating oxygen ions. Previous experimental work on related materials supports the MD results (please refer to Fig. 11 of ref. 14). $La_2CoO_{4+\delta}$ is another potentially important RP compound for oxide ion conduction[81–83] (Table 1), and the oxygen conduction mechanism in it is characteristically the same as the path described here. For $La_2CoO_{4+\delta}$, the differences in the computationally predicted and the experimentally measured migration barriers, which involve both experimental and computational uncertainties, are discussed in depth by Kushima *et al.*[81] As summarized here, the facile migration of the interstitial oxygen in these RP compounds is enabled by the cooperative titling–untilting of the $(Ni,Co)O_6$ octahedron, and exemplifies the role of lattice flexibility in reducing the barriers to oxygen diffusion.

5.2. Layered double perovskites

Ordered double perovskites with general formula $AA′B_2O_{5+\delta}$, where A = rare earth, A′ = alkaline earth and B = Co, Mn, have been recently proposed as next generation Intermediate

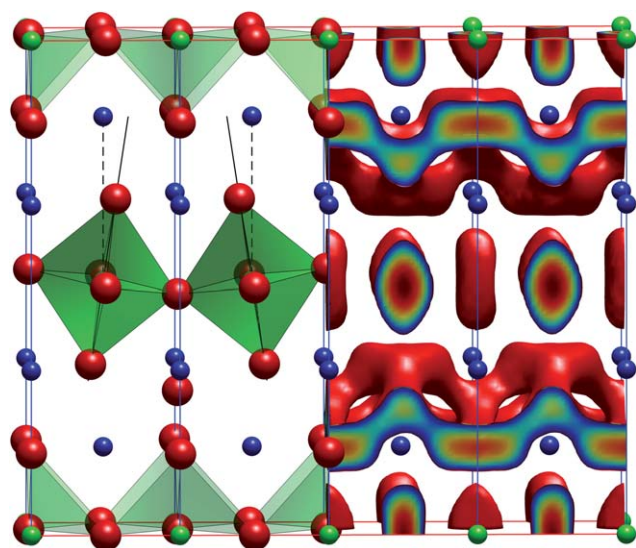**Fig. 3** The tetragonal crystal structure of $Pr_2NiO_{4+\delta}$ (O in red, NiO_6 octahedra in green and Ni in blue) and the isosurface connecting the O diffusion sites in the a–b plane (the c-axis in the vertical axis) from the MD calculations of Parfitt *et al.*[80] at 1100 K and $\delta = 0.09875$. Note the distortion of the NiO_6 octahedra away from the oxygen interstitial (reproduced from ref. 80 by permission of PCCP Owner Societies).

Fig. 4 The diffusion coefficient with respect to the oxygen hyper-stoichiometry, δ, in $Pr_2NiO_{4+\delta}$ (reproduced from ref. 80 by permission of PCCP Owner Societies).

Temperature-SOFC (IT-SOFC) cathode materials due to their high electronic conductivity (above the metal–insulator transition temperature, 300–400 K),[84] remarkable oxygen mass transport properties[12,16,17] (lowered activation energy compared to most of the simple perovskite cathodes[6]) and excellent performance when integrated in fuel cell devices.[85–93]

These double perovskite materials are derived from aliovalent substitution on the A-site of a simple perovskite oxide (ABO_3), with general formula, $A_{0.5}A'_{0.5}BO_{3-\delta}$, which generates oxygen vacancies. For a significant size mismatch between the two A-site cations, the simple perovskite structure tends to adopt a layered arrangement due to an A-site cation ordering and the formula for the material is then rewritten in the double perovskite manner, $AA'B_2O_{5+\delta}$ (Fig. 5).

This particular structural feature is in the origin of the excellent oxygen mass transport properties already reported in the literature. For the particular case of $GdBaCo_2O_{5.5}$ (GBCO), Parfitt *et al.*[88] and Hermet *et al.*[89] carried out first MD simulations shedding some light on the oxygen transport mechanisms and their correlation with the structure and the observed
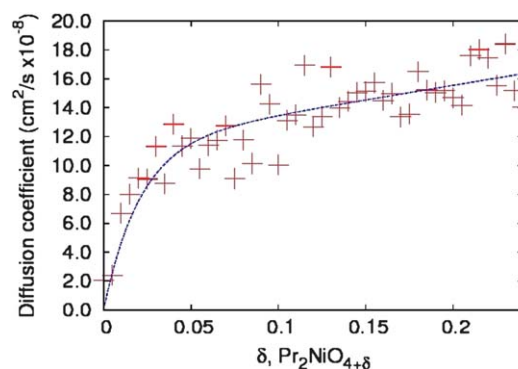
macroscopic properties. In these independent works, MD simulations were able to reproduce the high diffusivities and low activation energies experimentally measured by isotopic exchange techniques (Fig. 6 and Table 2). The simulations showed anisotropic oxide ion conduction based on pathways through Gd-, Co- and O-sites (Fig. 7). This direct visualization of an anisotropic diffusion is consistent with experimental results, based on diffraction of $LnBaCo_2O_{5+\delta}$ (Ln = Pr, Gd) compounds, which determined lower occupancy for the oxygen sites in the $[LnO]_\delta$ plane at high temperatures.[90,91]

High diffusivity and low values of activation energy reported for this family of compounds are quite unexpected since heavily doped structures, such as these aliovalent substituted double cobaltites, usually suffer from association between dopants and oxygen vacancies that reduces the oxide ion mobility, *e.g.* the ionic conductivity is depressed for heavily doped fluorites or pyrochlores,[92] as discussed in section *Diffusion mechanisms*. However, MD simulations in these systems have showed that the existence of an ordered cation sublattice avoids trapping effects allowing a highly disordered oxygen sublattice. The characteristic layered structure restricts the ionic conduction to the most favorable conduction planes, avoiding diffusion along planes containing the largest cation (Ba^{2+}), *i.e.* the cation with highest coordination number. In this direction, Parfitt *et al.*[88] investigated the effect of cation ordering in the oxygen mass transport of GBCO by introducing controlled disorder in the A-site, ranging from total disorder to layered compounds. A continuous increase of the oxygen diffusivity perpendicular to the conduction plane is observed for a higher level of disorder until an

Table 1 Activation energies of oxygen self-diffusion in $A_2BO_{4+\delta}$. In the modeling studies the direction of migration is the a–b plane

| Material	E_d/eV	Methodology	Comment	Reference
$La_2CoO_{4+\delta}$	0.12	Experimental		82
$La_2CoO_{4+\delta}$	1.27	DFT	Interstitial mechanism	81
$La_2CoO_{4+\delta}$	0.73	DFT	Interstitialcy mechanism	81
$La_2CoO_{4+\delta}$	0.47	MD	Interstitialcy mechanism	81
$Pr_2NiO_{4+\delta}$	0.49–0.64	MD	Interstitialcy mechanism	80
$La_2NiO_{4+\delta}$	0.51	MD	Interstitialcy mechanism	79
$La_2NiO_{4+\delta}$	1.2	DFT	Interstitial mechanism	15
$La_2NiO_{4+\delta}$	0.19	Experimental	Epitaxial thin film	18
$La_2NiO_{4+\delta}$	0.54	Experimental	Polycrystal, TOF-SIMS	30
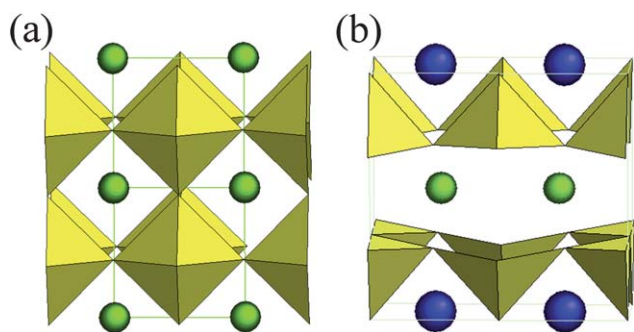
Fig. 5 Polyhedral view of (a) simple perovskite structure of $GdCoO_3$ and (b) high temperature ordered double perovskite structure of $GdBa\text{-}Co_2O_{5+\delta}$ (*P4/mmm* space group). In the layered perovskite structure, Co ions are coordinated in pyramids (CoO_5) and octahedra (CoO_6) with oxygen vacancies along Gd (light green) planes. Blue spheres represent Ba.

isotropic diffusion is achieved. Furthermore, the total diffusivity dropped to a third of the ordered case for the fully disordered system suggesting that the most favorable structure in terms of oxygen mass transport is the ordered one. This result is in accordance with the experimental results based on oxygen uptake kinetics in oriented single crystals[94] that showed a significant improvement of the oxygen transport properties induced by cation ordering taking place in similar compounds ($Gd_{0.5}Ba_{0.5}MnO_{3-\delta}$ compared to $GdBaMn_2O_{5.5}$).

As previously suggested by Norby,[94] cation ordering can provide highly percolative pathways for oxygen migration in heavily substituted compounds if the anion sublattice disorder is not altered, *i.e.* the equivalency of all the anion sublattice sites is preserved. Since dopant cations extensively associate to vacancies, efficiently fixing these dopant traps in positions out of the percolation paths will increase the ionic conductivity. This promising strategy can be of the utmost importance if keeping the cation ordering is possible even for systems where dopants tend to segregate to grain boundaries and interfaces blocking the oxide ionic conduction, with the consequent lower performance
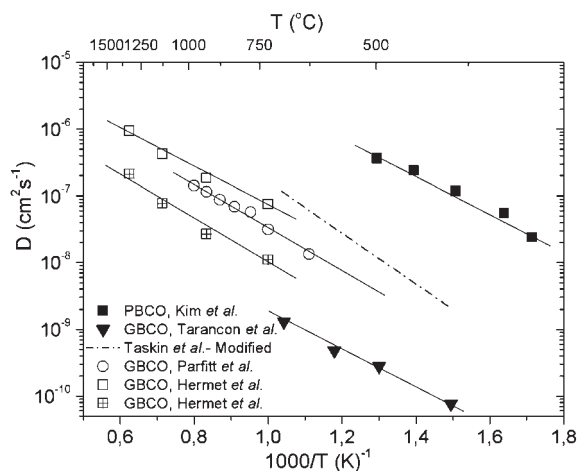

Fig. 6 Arrhenius plot of calculated (open symbols) and experimentally measured (closed symbols) oxygen diffusivities for ordered double perovskites.[12,16,17,88,89]

of the final device.[95,96] Simulations can help in reaching an overall understanding of the optimum trade-off between stable ordered structures and highly percolative disordered oxygen sublattices.

At this stage only limited experimental data on a small number of compositions with ordered double perovskite structure are available.[6] Therefore, the scope for optimizing their performance is enormous, especially if we consider mixed occupancy of both A and B cation sites. The use of atomistic simulations can play an important role in mapping out and acquiring a fundamental understanding of the effect of the nature of the A, A′ and B cations on the conduction and catalytic properties.

5.3. Other examples to layered oxides

There are a number of perovskite-related layered oxides that have been proposed or are presently being investigated as cathodes for SOFCs.[97–110] Of particular importance are the iron, copper and cobalt containing perovskite-related oxides.[6,105] The mechanism and energetics of oxygen transport in most of these materials is a relatively unchartered area because of the immense number of possible combinations due to differences in composition, stoichiometry, and crystal structure. Sometimes the accurate experimental determination of the oxygen diffusion process in ceramic samples can be hindered by grain boundaries or other artifacts and therefore an atomistic simulation approach becomes extremely useful. For example, experimental work on $Sr_4Fe_6O_{13}$ ceramic did not determine significant ionic conductivity[107–109] in contrast to the simulations of Fisher and Islam[87,110] that predicted a better ionic conductivity than the parent $Sr_2Fe_2O_5$, due to energetically favoured oxygen diffusion paths in particular crystallographic directions. Although the origin of the low conductivity in pure ceramic $Sr_4Fe_6O_{13}$ is still in controversy, it is likely due to blocking effects associated to the grain boundaries present in polycrystalline samples. Experimental measurements on single crystals are required for clarifying this issue. This particular case highlights how atomistic simulation can help and guide in overcoming experimental limitations by covering fundamental aspects of oxygen diffusion mechanisms in greater detail and accuracy.

Cobalt oxides are another potentially important category of materials that can be used as cathodes for SOFCs, oxygen separation membranes and other applications.[111–113] The structure and properties of $Sr_{1-x}Ln_xCoO_{3-\delta}$ ($Ln =$ Y, rare-earth cations) have received considerable attention.[111–113] For example, $Sr_{0.7}Y_{0.3}CoO_{2.62}$ was determined by Istomin *et al.*[114] to exhibit the tetragonal symmetry (space group *I4/mmm*, no. 139). Interestingly, in $Sr_{0.7}Y_{0.3}CoO_{2.62}$ the layers of CoO_6 octahedra alternate with the oxygen deficient layers (see Fig. 8; similar to the Brownmillerite structure reviewed among Electrolyte Materials in the following section). It is of importance that one of the oxygen sites (the O4, Fig. 8) has a partial occupancy of $^1/_4$, with only one of the four adjacent positions being occupied. In a recent MD study Rupasov *et al.*[115] investigated the oxygen diffusion mechanism in $Sr_{0.75}Y_{0.25}CoO_{2.625}$. The calculations revealed that oxygen diffusion both in the *a–b* plane and along the *c*-axis requires equivalent rate-limiting ion hops. Therefore, oxygen diffusion in $Sr_{0.75}Y_{0.25}CoO_{2.625}$ is isotropic with an activation energy of 1.56 eV in the temperature range 1000–1400 K.[115] This activation energy is in excellent agreement with the

Table 2 Comparison of oxygen diffusivity data (chemical diffusion) obtained by both isotopic diffusion measurements and MD calculations for ordered layered perovskites
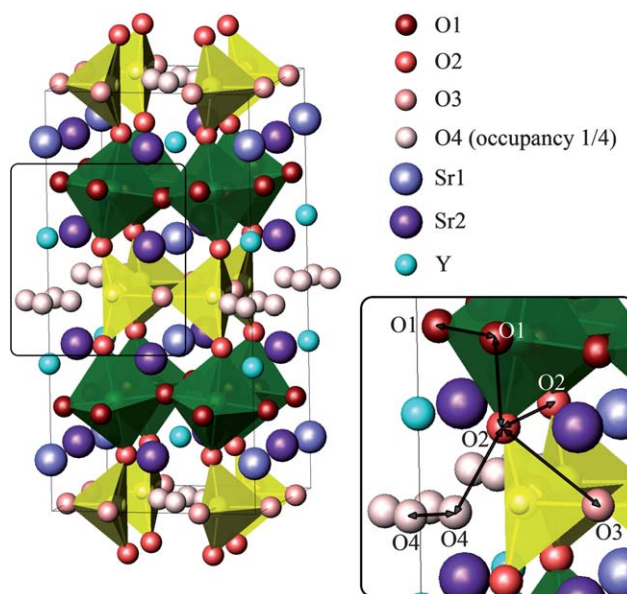
	D^*/cm^2 s^{-1} $T = 500$ °C	E_a/eV	Method	Ref.	Notes
GdBaCo$_2$O$_{5+\delta}$	1.2×10^{-8}	0.70	Weight change	12	Modified values according to ref. 17
GdBaCo$_2$O$_{5+\delta}$	2.8×10^{-10}	0.60	Isotopic exchange	17	
PrBaCo$_2$O$_{5+\delta}$	3.6×10^{-7}	0.48	Isotopic exchange	16	
GdBaCo$_2$O$_{5.5}$	3.1×10^{-9}	0.50	MD	88	Diffusivity from extrapolation
GdBaCo$_2$O$_{5.5}$	1.2×10^{-9}	0.67	MD	89	Diffusivity from extrapolation
GdBaCo$_2$O$_{5.5}$	1.5×10^{-8}	0.56	MD	89	Diffusivity from extrapolation
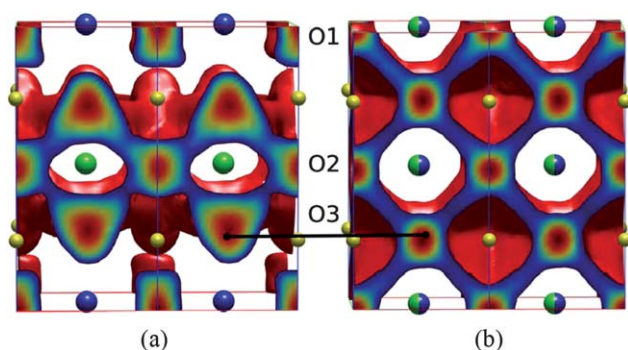
Fig. 7 Calculated oxygen density profiles obtained by MD for (a) an ordered and (b) a fully disordered perovskite with formula, GdBaCo$_2$O$_{5.5}$. This visualization shows the anisotropic oxygen diffusion for ordered double perovskites. Green and blue spheres represent Gd and Ba respectively. Three different oxygen positions can be defined and are labeled O1, O2, O3 (reproduced from ref. 88).

Fig. 8 The crystal structure of Sr$_{0.7}$Y$_{0.3}$CoO$_{2.62}$. The CoO$_6$ octahedra layers alternate with oxygen deficient layers (O3, O4) and CoO1 atoms.[115]

experimental value of about 1.5 eV that was determined after the MD investigations.[116]

6. Oxygen transport mechanisms in electrolytes

Desirable properties for an electrolyte are high ionic conductivity, low electronic conductivity, chemical and mechanical compatibility with the electrode materials, and phase stability in both oxidizing and reducing conditions. Enabling fast oxide ion transport in electrolyte materials is essential to facilitate the intermediate- to low-temperature operation of SOFCs for enhanced durability and economics. The ultimate choice of the oxide ion electrolyte for the intermediate temperature SOFCs is not yet clarified. The focus of this section is the oxygen ion transport mechanisms and diffusivity in a representative set of electrolyte materials. We first summarize the ionic transport mechanisms in the electrolyte materials which are widely studied and in some respects are regarded as conventional or *old* although the duly excitement about them never vanishes. We then exemplify non-traditional anion transport paths from recent studies, focusing on the role of *lattice flexibility and dynamics*. Lastly, we come back to the *old* materials, and highlight the new developments in the potential to increase the ionic conductivity in them. For this, we highlight the experimental and theoretical studies in which the oxide materials are subjected to external mechanical stimuli, bringing about the *mechano-chemical* coupling in potentially driving fast ionic transport. The strength of this coupling also stands for the lattice/bonding *flexibility* in the oxides. A mechanistic understanding of oxygen transport from atomistic details in these families of oxides, and of how oxygen transport can be manipulated by external mechanical stimuli, are important for developing strategies for increasing the oxygen ion conductivity in next-generation materials and microstructures for SOFCs.

6.1. Cubic systems with oxygen ion hopping

The three most widely investigated electrolyte systems are yttria stabilized zirconia (YSZ), gadolinium- or samarium-doped ceria (CGO or CSO), and strontium- and magnesium-doped lanthanum gallate (LSGM).[3,51,117–119] The zirconia- and ceria-based electrolytes have fluorite crystal structures, with the cations occupying the fcc lattice sites and the O^{2-} ions occupying the tetragonal sites. LSGM is a perovskite oxide, with the O^{2-} ions occupying the face centers, forming (Ga,Mg)O$_6$ octahedra, and with the (La,Sr) cations on the corner sites. Both structures are shown in Fig. 2. The commonality among these cubic symmetry solids is that the oxygen anion transport is mediated by anion vacancies, and takes place by the thermally activated hopping of an anion from one site to the nearest anion vacancy site.[51,92] This leads to a vacancy flux and an anion flux of opposite directions. At the intermediate temperature range, the energy barriers for this mechanism are typically high to enable fast diffusion, and among these three conventional electrolyte

systems, the oxygen ion conductivity of YSZ is the lowest, and that of CGO is the highest.[120–122] The migration paths of an oxygen anion in the fluorite and the perovskite structures are shown in Fig. 2, exemplifying the case for YSZ and CSO/CGO in (a,b), and for LSGM in (c,d).

As discussed in Section 3, the barrier for the thermally activated vacancy migration paths is the critical descriptor for how low a temperature the electrolyte can effectively function at. A change in the migration barrier, E_B, affects D_v, and consequently D_0 exponentially (eqn (2)–(4)). The reported migration barriers for oxygen anion transport range as 1.0–1.2 eV in YSZ, 0.9–1.16 eV in CGO, and 0.79 eV in LSGM.[123] The limits of ionic conductivity in the context of vacancy mediated transport in these cubic symmetry systems depend directly on the bond strength between the oxygen and the neighbouring cations, which is influenced by the local defect–defect interactions. In the last section, we will come back to these *old* electrolyte materials as noted here, and present the new developments in identifying *mechano-chemically* coupled ways to reduce the energy barriers to oxygen migration in these rather well-known systems. In the next section, we highlight structures which do not rely on oxygen ion hopping for oxygen transport, but rather on the flexibility of the lattice.

6.2. Non-cubic, anisotropic systems with lattice dynamics

There are a number of recently described transport paths for oxygen transport to take place *via* intercalation at lower temperatures. First principles-based and atomistic simulations have been instrumental in discovering such new mechanisms. Two primary structure types that intercalate oxygen fast belong to the oxygen deficient Brownmillerite structure, and structures containing *active* tetrahedral moieties as the oxygen excess apatite. These are not cubic, and possess anisotropic paths of oxygen conduction. In particular, *lattice dynamics* characterized by the significant relaxation and cooperative motion of local polyhedra assists the conduction of oxygen atoms, without necessitating an oxygen ion/vacancy hopping path as discussed above for the cubic systems.

(1)   Brownmillerites. $BaInO_{2.5}$, $CaFeO_{2.5}$ and $SrFeO_{2.5}$ are example compositions in this structure family for oxygen ion conduction.[124,125] The key characteristic of the Brownmillerite structures is the alternating octahedral and tetrahedral layers, and the 1D ordered vacancy channels in the tetrahedral layers at lower temperatures. At high temperatures, for example above 925 °C for $BaInO_{2.5}$, the oxygen vacancies disorder and the symmetry becomes tetragonal.[126] It transforms to a disordered cubic form at 1040 °C. It is debated that the disorder induced in the oxygen sublattice leads to high ionic conduction at these higher temperatures. On the other hand, it was also shown that the vacancy ordered channels can fill up, through fast diffusion, completely already at room temperature in $SrFeO_{2.5}$, to form eventually the cubic perovskite.[127,128] The underlying atomistic mechanism for this unusually fast oxygen transport kinetics at low temperatures in Brownmillerites was revealed recently using inelastic neutron scattering and *ab initio* molecular dynamics.[129] In summary, the apical oxygen atoms can exhibit large displacements, and if they get sufficiently far from their equilibrium positions, they are able to escape into the vacancy channels of the tetrahedral layer. The structure left behind is then a square pyramid, and a reoriented tetrahedron (see Fig. 9(a) and (b) for $SrFeO_{2.5}$), signifying the ability of the lattice to dynamically accommodate multiple polyhedral configurations. A pronounced lattice dynamics exists for the tetrahedral chains, showing a marked zig-zag switching behavior. The potential of the apical oxygens to do this is mainly determined by the Fe–O bond strength and length along the *c*-axis; the longer the bond, the easier to displace the oxygen atom. Therefore, the possibility of this fast kinetics strongly depends on the lattice parameter along the *c*-axis. The same path was found experimentally to be much slower and active only at higher temperatures in $CaFeO_{2.5}$ (above 700 K, *vs.* 600 K for $SrFeO_{2.5}$),[129] whose *c*-axis lattice parameter is shorter than that of $SrFeO_{2.5}$ ($c_{CaFeO_{2.5}} = 14.77$ Å and $c_{SrFeO_{2.5}} = 15.85$ Å).[129,130] While these Fe-containing Brownmillerites would also be electronically conducting, rendering them more suitable as a cathode, the oxygen conduction path in these structures could be representative of also the purely ionic conducting $BaInO_{2.5}$ at low temperatures as a candidate electrolyte material.

(2)   Active tetrahedral moieties. Structures containing tetrahedral moieties such as $La_{1-x}Ca_xMO_{4-x/2}$ (M = Ta,Nb,P), $La_{1-x}Ba_{1+x}GaO_{4-x/2}$, and $La_{9.33+x}Si_6O_{26+3x/2}$, have been attracting considerable attention for fast oxygen transport.[131–133] We review two examples demonstrating the role of lattice flexibility and dynamics, with significant relaxations of the tetrahedral moieties, rendering them *active*, in enabling an almost hand-to-hand transfer of the oxide ions.

(i)   Taking the $La_{1-x}Ba_{1+x}GaO_{4-x/2}$ as a model system, Kendrick *et al.*[134] recently elucidated the atomic scale oxygen conduction mechanism in these systems using a combined experimental and computational modelling approach. The structure of $LaBaGaO_4$ contains gallium in a distorted tetrahedral environment and ordered alternating layers of lanthanum and barium. The gallate tetrahedra are identified as isolated moieties within the lattice. Upon removal of an oxygen from a GaO_4 unit, rather than producing a three-coordinate Ga unit, considerable relaxation of a neighbouring GaO_4 unit takes place. A Ga_2O_7 group is formed, such that each Ga retains a tetrahedral coordination, sharing one apical oxygen between two tetrahedra (Fig. 10(a)). The prediction of such Ga_2O_7 defects from the modeling work was also supported by the neutron diffraction data for the 'dry' $La_{0.8}Ba_{1.2}GaO_{3.9}$ sample. The data showed a spread of nuclear density along the *c* axis with a split oxygen site, which is consistent with the presence of both an isolated GaO_4 tetrahedron and a Ga_2O_7 unit. The oxide-ion conduction in this system then proceeds *via* a cooperative 'cog-wheel'-type process involving the breaking and re-forming of Ga_2O_7 units (Fig. 10(b)). Local lattice relaxation around the migrating ion is a key enabler for this process. The minimum energy pathway for the oxygen migration was shown to occur *via* the breaking and re-formation of the Ga_2O_7 units, with an effective oxide-ion migration energy of 0.59 eV. The transfer of oxide ions between neighbouring tetrahedra facilitates long-range diffusion. While this is an unusual mechanism for ceramic oxide materials, similar cooperative processes with lattice dynamics may be important in related systems containing tetrahedral moieties.
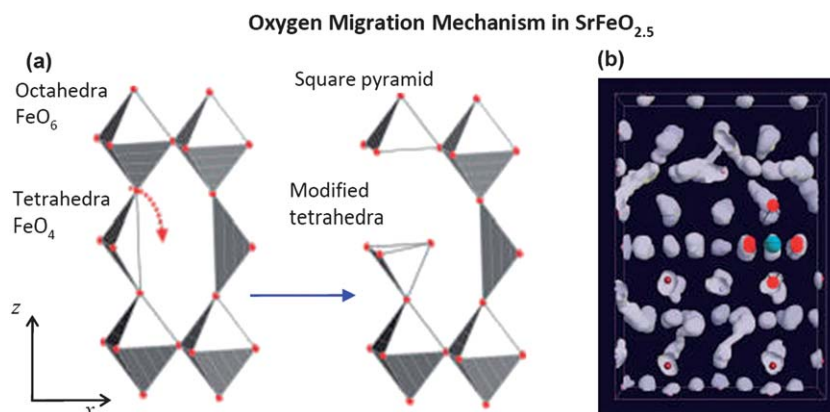
Oxygen Migration Mechanism in SrFeO₂.₅

(a)

Octahedra
FeO₆

Square pyramid

Tetrahedra
FeO₄

Modified
tetrahedra

(b)

Fig. 9 (a) SrFeO$_{2.5}$, Brownmillerite framework, before and after the diffusion of an apical oxygen atom (shown by red dashed arrow) yielding a FeO$_5$ square pyramid, and a modified FeO$_4$ tetrahedron. (b) Atomic trajectories along a 10 ps *ab initio* molecular dynamics run at 350 K (oxygen positions are red spheres), where the apical oxygens follow a zig-zag pattern dynamics (reprinted with permission from ref. 129).

(ii) *Apatites* with the general formula $Ln_{10}(XO_4)_6O_{2\pm y}$, where Ln is a rare-earth or alkaline earth metal, and X is P, Si or Ge, have high oxygen conductivity.[135–139] Fig. 11(a) illustrates the structure of the apatite La$_{9.33}$(SiO$_4$)$_6$O$_2$. In this the isolated SiO$_4$ tetrahedra are arranged in such a way that they form two distinct channels parallel to the *c*-axis. Lanthanum cations occupy both of these channels, whereas oxygen ions reside in the larger channel (Fig. 11(a)). Interestingly, in apatites oxygen transport is *via* an interstitial mechanism, with the importance of oxygen interstitials being highlighted in previous experimental studies.[133,140–142] The atomic scale modelling work of Tolchard *et al.*[138] predicted that the interstitial oxygen resided in the periphery of the larger channel and not at its centre. This arrangement is energetically favourable as the neighbouring SiO$_4$ tetrahedron is displaced towards the La channels. Thereafter, experimental evidence[133,141–143] verified the calculations of Tolchard *et al.*[138]

As expected by the channels existing in its structure oxygen diffusion in La$_{9.33}$(SiO$_4$)$_6$O$_2$ is highly anisotropic and prevalent

along the direction of the channels (*c*-axis). Atomistic simulation studied by Kendrick *et al.*[133] revealed that the oxygen diffusion follows a sinusoidal path (Fig. 11(b)). The oxygen transport involves the cooperative displacements of the SiO$_4$ tetrahedra, as described above in (*i*) and Fig. 11, and their flexibility and dynamics are thus very important.[133] Apatites can exhibit a wide range of oxygen or cation stoichiometries and can readily incorporate dopants.

6.3. Emerging opportunities through interfaces and lattice strain in nanoscale structures

Besides the conventional approaches of searching for novel structures and compositions, or of altering oxygen and cation stoichiometry, introduction of dissimilar interfaces is a potentially powerful method of modifying the ionic transport properties of ceramics.[144] The tremendous sensitivity of the properties of oxides to strain and defects is greatly amplified at interfaces,[145] resulting in significant and quantifiable effects on charge-carrier

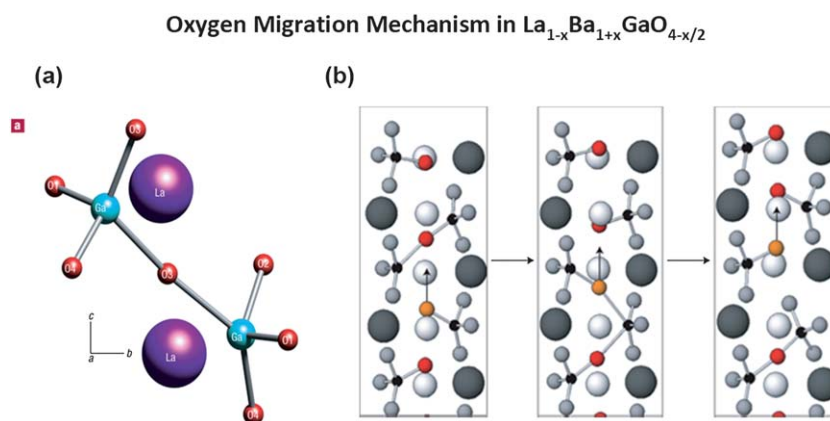## Oxygen Migration Mechanism in La₁₋ₓBa₁₊ₓGaO₄₋ₓ/₂

(a)

(b)

Fig. 10 (a) Local structure around an oxide-ion vacancy defect in the LaBaGaO$_4$ system. Considerable local relaxation takes place upon removal of an oxide ion, forming a Ga$_2$O$_7$ unit. Removal of an oxide ion from one GaO$_4$ tetrahedron causes a neighboring tetrahedron to share one of its anions so that both maintain four-fold coordination. This requires slight rotation of both gallium–oxygen moieties. (b) Oxygen vacancy migration pathway in La$_{1-x}$Ba$_{1+x}$GaO$_{4-x/2}$. The transport mechanism involves the formation and breaking of Ga$_2$O$_7$ units along the migration pathway. The transfer of oxide ions between neighboring tetrahedra "from hand to hand" enables long-range diffusion to take place. The migrating oxide ions are highlighted in yellow (reprinted with permission from ref. 134).
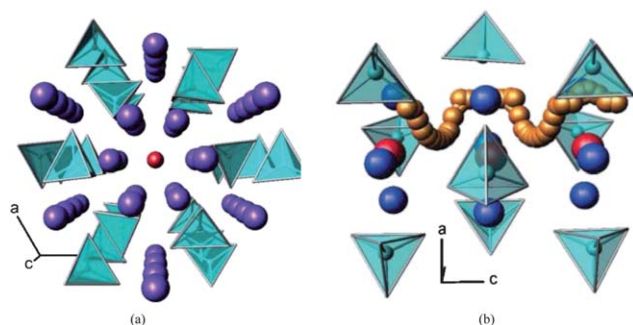
Fig. 11 (a) The structure of the apatite La$_{9.33}$(SiO$_4$)$_6$O$_2$ and (b) the oxygen migration path (yellow) perpendicular to the *c*-axis. Channel oxygen ions in red, SiO$_4$ tetrahedra in light blue and La cations in purple (reproduced from ref. 133).

density and mobility. The strain state at and near the interface can alter the electronic structure and bond strengths to provide for improved charge transfer,[146] and improved ion mobility.[147] The ability to tune the atomic-level structural and chemical state of the interfaces and near-interface regions to favour fast oxygen transport in SOFC electrolytes, as well as in electrodes, is of high importance.[148] Here, for this purpose, we turn our attention to the anisotropic lattice strains. Surface strain effects have received significant excitement for accelerating low temperature electrocatalysis rates on transition metals since the report by Mavrikakis *et al.*[146] in 1998. On the other hand investigations of lattice strain effects on defect chemistry, ionic transport and reactivity in oxides are yet scarce, with recent results indicating a potentially significant impact in favorably altering the ionic transport rates in SOFC-relevant materials.[38,149,150] Generalized theoretical and experimental strategies making use of strain states in controlling the ionic transport and reactivity of ceramics do not yet exist. Here we present the recent findings on the mechanistic and quantitative effects of biaxial lattice strain in accelerating the oxygen ion transport in electrolyte materials, as a prime example for *mechano-chemical coupling* in ceramics. The results are drawn from recent theoretical and experimental work on YSZ. In this way, we hope to give some guidance on how nanoscale structures can be devised to enable fast oxygen transport upon mechanical stimulation. The most important message to take away is the potential of the lattice strain to reduce the oxygen migration energy barriers, which is a key factor for enabling fast oxygen transport as we noted in Section 3.

The "fastest strain" in yttria stabilized zirconia. An eight orders of magnitude increase in conductance of 1–30 nm thick yttria stabilized zirconia (YSZ) layers coherently "strained" between dielectric SrTiO$_3$ (STO) layers, as reported by Barriocanal *et al.*,[36] sparked great interest in this system. To date, the exact nature of the ionic *versus* electronic conductance induced in the vicinity of the YSZ/STO interface remains debatable.[147] Theoretical efforts following this experimental report dug deeper into the mechanisms of what lattice strain alone can do to the oxygen transport in bulk YSZ, regardless of the electronic and space charge effects that can arise at the YSZ/STO interface. In assessing the role of biaxial tensile strain with atomistic details, Kushima and Yildiz combined first principles-based calculations

of migration paths and barriers, with kinetic Monte Carlo-based atomistic calculations of effective diffusivity.[38] As a result, they identified that two competing and non-linear processes acting in parallel alter the migration barrier for oxygen upon applied strain. First, at low strain states where elastic stretching of the cation–oxygen bonds prevails, the increase of the migration space and the weakening of the local oxygen-cation bonds decrease the migration barrier. With the decrease in the migration barrier, the oxygen diffusivity exhibits an exponential increase up to a critical value of tensile strain, namely the *fastest strain*. This increase is more significant at the lower temperatures. Second, at strain states higher than the critical strain the diffusivity decreases, because the local relaxations at large strains break and re-form bonds (Fig. 12) and trap the oxygen by strengthening the local oxygen-cation bonds and increase the migration barrier. This is transition to local plastic relaxations. Yildiz and Kushima consider ten representative migration paths for oxygen in 9%-YSZ, taking into account the vacancy and dopant configurations near the migration path, including those beyond the first and second nearest neighbours.[38] The electronic charge density distribution on the cation–oxygen (C–O) bonding plane along one such migration path in YSZ is shown in Fig. 12 as a function of strain. For the particular vacancy migration path in Fig. 12, the elastic stretching up to 6% strain weakens the cation–oxygen bond (marked as C and O) and reduces the migration barrier of oxygen (marked as O) towards the vacancy on the left. From 6% to 8% strain, the breaking of a neighbouring cation–oxygen bond upon local relaxations re-strengthens the C–O bond, and increases the migration barrier again. The highest effective enhancement of diffusivity in 9%-YSZ compared to its unstrained state is at 4% as the fastest strain, by 7 × 10^3 times at 400 K and by 3 × 10^1 times at 1000 K (Fig. 13). The effective migration barrier is reduced by 0.4 eV. One could view this *fastest strain* as the optimal strain state to induce in the material system in order to attain the maximum benefit of the biaxial lattice strain on the oxygen diffusivity.

Using a higher level phenomenological model based on the elastic properties of YSZ, Schichtel *et al.* estimated a 2.5 orders of magnitude increase in the ionic conductivity of YSZ at 7% strain at 573 K. Schichtel *et al.*'s[150] model relies on the isotropic pressure induced by elastic strain to enhance the diffusivity, and does not take into account the microscale competing elastic-to-plastic relaxations at these large tensile strain states in YSZ. Therefore, it cannot capture the strain dependence of the local bond-strengths and migration energies, which may mitigate the diffusivity at large strain values beyond elastic stretching. In spite of the differences in Schichtel *et al.*'s and Kushima and Yildiz's models, the magnitude of the maximum relative increase in the oxide ion diffusivity in strained YSZ predicted by these models range from 2.5 to 3.8 orders of magnitude. Such potential increase is significant by itself. On the other hand, the lattice strain (elastic and plastic) alone cannot explain an eight orders of magnitude increase of ionic conductivity in YSZ as reported by Barriocanal *et al.*[36]

Interestingly Sillassen *et al.*'s[35] more recent experiments on 58 nm thick epitaxial YSZ films on MgO also show very high lateral ionic conductivities, and agree with the quantitative predictions of Kushima and Yildiz. The enhancement in ionic conductivity is especially significant at the low temperatures (<350 °C), by more
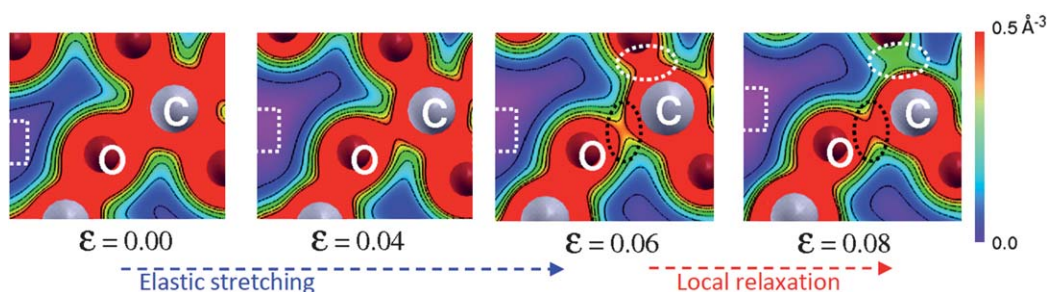
Fig. 12 The electronic charge density distribution on the cation–oxygen (C–O) bonding plane in YSZ as a function of biaxial lattice strain, ε, from 0.00 to 0.08, at the initial configuration of the oxygen migration. Weakening of the O–C bond upon elastic stretching up to $\varepsilon = 0.06$ corresponds to the decrease of the migration barrier. Re-strengthening of the O–C bond (black dashed oval), in concert with the breaking of a neighbouring cation–oxygen bond (white dashed oval) upon local relaxation from $\varepsilon = 0.06$ to 0.08, increases the migration barrier again. Gray and red spheres represent Zr and O atoms, respectively. White dashed square is the location of the oxygen vacancy, and oxygen marked as O is the migrating oxygen towards the vacancy. The isoline-interval is 0.5 Å^{-3} (adapted from ref. 38).

than 3.5 orders of magnitude compared to bulk YSZ, and is accompanied by a reduction in the effective activation energy from 1.24 eV for bulk YSZ to 0.89 eV for the epitaxial YSZ films on MgO at the lower temperatures. The relative reduction in the activation energy, the order of magnitude of the increase in ionic diffusivity, and the significance of this increase at lower temperature are consistent with and support the predictions of Kushima and Yildiz discussed above.[38] Sillassen *et al.*[35] attribute the increase in the conductivity at lower temperatures to the YSZ-substrate interfacial effects, induced by a combination of misfit dislocation density and elastic strain at the interface. We think that, even in the case of the misfit dislocations, the elastic strain field around the misfit dislocations can reduce the migration barriers and enable fast ionic transport, in the same way as the model described by Kushima and Yildiz.[38]

These very high oxide ion conductivities proposed by experiments and theory in the *conventional* YSZ composition, put into an *unconventional* structure in the form of strained thin films, are of great fundamental importance for fast ionic transport. The theoretical gains from lattice strain in these oxides are exponential in altering the diffusion kinetics, thanks to the flexible stretching of the cation–oxygen bonds. Even in the context of plastically deformed oxides which possess dislocations, each dislocation is associated with an elastic strain zone (tensile and compressive) around itself. Therefore, the discussion here on the

enhancement of ionic diffusion with lattice strain can also apply to elastic strain zones around the dislocations. Taking advantage of *mechano-chemical* coupling to induce such high conductivities can also be technologically relevant for low-temperature SOFC applications. This is yet another example of how structural flexibility, here as elastic stretching, can enable more facile oxygen transport. Systematic experimental and theoretical investigation of the role of local strain states on tuning the mechanism and magnitude of ionic conduction properties in these solid state ionic materials is prone to pursuit of an exciting and promising research and development path.

7. Conclusions and future outlook

Diffusion is a fundamental unit process that is highly important in the field of solid state ionics. This perspective article has highlighted the role of computational materials in predictively investigating the oxygen transport mechanisms and energetics in complex oxides as SOFC-relevant materials. The need for new materials is driven by the requirement that cathode materials operate efficiently (catalyze the oxygen reduction reaction) at lower temperatures and electrolytes with better ionic conductivity, stability and mechanical properties. An approach based on predictive simulations is necessary in accelerating the identification or design of appropriate materials. In combination with
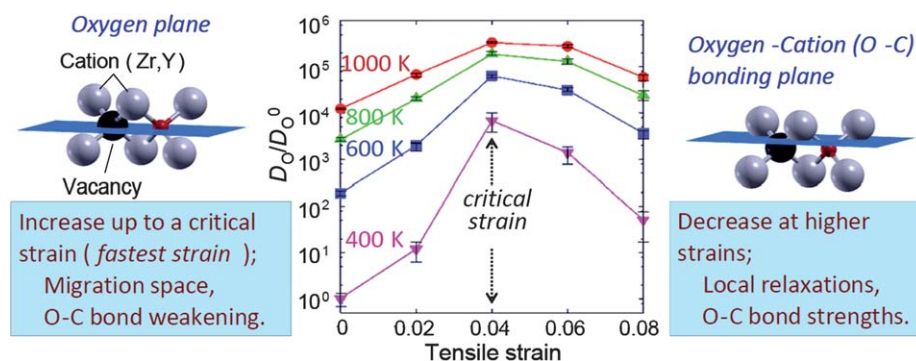

Fig. 13 Two competing factors alter the oxygen migration barrier upon applied strain in Y$_2$O$_3$ stabilized ZrO$_2$ (YSZ): (1) space along the migration path, and (2) bond strength between the migrating oxygen and its nearest neighbour cations (O–C bond). The maximum relative enhancement in oxygen diffusivity (D_o/D_o^0) was 6.8×10^3 times at 4% strain at 400 K (adapted from ref. 38).

validation and verification experiments, computational approaches at the first principles and atomistic scales are replacing empirical qualitative arguments in the discovery of new materials in a rational and efficient way.

This article focused on recent results through direct atomic scale insights on the oxygen ion conduction mechanisms and properties in potential cathode and electrolyte materials for SOFCs. The dependence of conduction path and ease is strongly linked to the local atomic structures. Among the new classes of materials, we reviewed layered perovskite-like oxides and structures with active polyhedra in enabling the oxygen transport. We highlighted non-traditional conduction paths with structural and transport *anisotropy* and *lattice flexibility/dynamics*, unlike the conventional vacancy-driven ionic conduction in traditional SOFC materials. As for the old materials, we showed that even they can be "stretched" to exhibit much faster oxygen transport. In *flex*-ing the old structures, cation–oxygen bond strengths can be controlled through lattice strain to enable easier migration of oxygen. This is a prime example of *mechano-chemical* coupling in complex oxides. As exemplified by the findings reviewed here, the ever increasing power of atomic scale computational techniques can be applied to probe the defect transport processes in SOFC materials at scales and complexity not previously accessible. The investigation of surfaces, interfaces and nanostructured materials is bound to be important in the years to come.[3] Nano-structured or nano-porous materials, apart form their technological application, will yield interesting diffusion phenomena as the strain density of interfaces and limited diffusion lengths will come into play.[144]

Acknowledgements

References

1 S. C. Singhal, *Solid State Ionics*, 2000, **135**, 305.
2 B. C. H. Steele and A. Heinzel, *Nature*, 2001, **414**, 345.
3 A. J. Jacobson, *Chem. Mater.*, 2010, **22**, 660.
4 N. Q. Minh and T. Takahashi, *Science and Technology of Ceramic Fuel Cells*, Elsevier, Amsterdam, 1995.
5 J. Fleig, *Annu. Rev. Mater. Res.*, 2003, **33**, 361.
6 A. Tarancón, M. Burriel, J. Santiso, S. J. Skinner and J. A. Kilner, *J. Mater. Chem.*, 2010, **20**, 3799.
7 S. B. Adler, J. A. Lane and B. C. H. Steele, *J. Electrochem. Soc.*, 1996, **143**, 3554.
8 S. B. Adler, *Solid State Ionics*, 1998, **111**, 125.
9 S. J. Skinner and J. A. Kilner, *Solid State Ionics*, 2000, **135**, 709.
10 E. Boehm, J. M. Bassat, P. Dordor, F. Mauvy and J. C. Grenier, *Solid State Sci.*, 2003, **5**, 973.
11 A. A. Taskin, A. N. Lavrov and Y. Ando, *Appl. Phys. Lett.*, 2005, **86**, 91910.
12 A. A. Taskin, A. N. Lavrov and Y. Ando, *Phys. Rev. B: Condens. Matter Mater. Phys.*, 2005, **71**, 134414.
13 I. Seymour, A. Chroneos, J. A. Kilner, and R. W. Grimes, in preparation.
14 E. Boehm, J. M. Bassat, P. Dordor, F. Mauvy, J. C. Grenier and Ph. Stevens, *Solid State Ionics*, 2005, **176**, 2717.
15 C. Frayret, A. Villesuzanne and M. Pouchard, *Chem. Mater.*, 2005, **17**, 6538.
16 G. Kim, S. Wang, A. J. Jacobson, L. Reimus, P. Brodersen and C. A. Mims, *J. Mater. Chem.*, 2007, **17**, 2500.
17 A. Tarancón, S. J. Skinner, R. J. Chater, F. Hernádez-Ramírez and J. A. Kilner, *J. Mater. Chem.*, 2007, **17**, 3175.
18 M. Burriel, G. Garcia, J. Santiso, J. A. Kilner, R. J. Chater and S. J. Skinner, *J. Mater. Chem.*, 2008, **18**, 416.
19 M. Yashima, M. Enoki, T. Wakita, R. Ali, Y. Matsushita, F. Izumi and T. Ishihara, *J. Am. Chem. Soc.*, 2008, **130**, 2762.
20 A. Chroneos, R. V. Vovk, I. L. Goulatis and L. I. Goulatis, *J. Alloys Compd.*, 2010, **494**, 190.
21 U. Schwingenschlögl, A. Chroneos, C. Schuster and R. W. Grimes, *Appl. Phys. Lett.*, 2010, **96**, 242107.
22 A. Chroneos, K. Desai, S. E. Redfern, M. O. Zacate and R. W. Grimes, *J. Mater. Sci.*, 2006, **41**, 675.
23 A. Chroneos, N. J. Ashley, K. H. Desai, J. F. Maguire and R. W. Grimes, *J. Mater. Sci.*, 2007, **42**, 2024.
24 A. Predith, G. Ceder, C. Wolverton, K. Persson and T. Mueller, *Phys. Rev. B: Condens. Matter Mater. Phys.*, 2008, **77**, 144104.
25 M. R. Levy, C. R. Stanek, A. Chroneos and R. W. Grimes, *Solid State Sci.*, 2007, **9**, 588.
26 A. Chroneos, H. Bracht, R. W. Grimes and B. P. Uberuaga, *Appl. Phys. Lett.*, 2008, **92**, 172103.
27 A. Chroneos, R. W. Grimes and H. Bracht, *J. Appl. Phys.*, 2009, **105**, 016102.
28 J. A. Kilner and J. T. S. Irvine, in *Handbook of Fuel Cells—Advances in Electrocatalysis, Materials, Diagnostics and Durability*, ed. W. Vielstich, H. A. Gasteiger and H. Yokokawa, John Wiley & Sons, 2009, vol. 5.
29 F. Mauvy, J. M. Bassat, E. Boehm, P. Dordor, J. C. Grenier and J. P. Loup, *J. Eur. Ceram. Soc.*, 2004, **24**, 1265.
30 R. Sayers, R. A. De Souza, J. A. Kilner and S. J. Skinner, *Solid State Ionics*, 2010, **181**, 386.
31 J. B. Goodenough, *Annu. Rev. Mater. Res.*, 2003, **33**, 91.
32 K. Huang, S. Ohara, H. Okawa, R. Maric and T. Fukui, *J. Alloys Compd.*, 2004, **303**, 454.
33 G. B. Zhang and D. M. Smyth, *Solid State Ionics*, 1995, **82**, 161.
34 S. Nakayama and M. Sakamoto, *J. Eur. Ceram. Soc.*, 1998, **18**, 1413.
35 M. Sillassen, P. Eklund, N. Pryds, E. Johnson, U. Helmersson and J. Bøttiger, *Adv. Funct. Mater.*, 2010, **20**, 2071.
36 J. C. Barriocanal, A. R. Calzada, M. Varela, Z. Sefrioui, E. Iborra, C. Leon, S. J. Pennycook and J. Santamaria, *Science*, 2008, **321**, 676.
37 A. Bogicevic and C. Wolverton, *Phys. Rev. B: Condens. Matter Mater. Phys.*, 2003, **67**, 024106.
38 A. Kushima and B. Yildiz, *J. Mater. Chem.*, 2010, **20**, 4809.
39 A. Bogicevic and C. Wolverton, *Europhys. Lett.*, 2001, **56**, 393.
40 T. H. Etsell and S. N. Flengas, *Chem. Rev.*, 1970, **70**, 339.
41 H. Inaba and H. Tagawa, *Solid State Ionics*, 1996, **83**, 1.
42 H. J. M. Bouwmeester and A. J. Burggraaf, in *Fundamentals of Inorganic Membrane Science and Technology*, ed. A. Burggraaf and L. Cot, Elsevier, Amsterdam, 1996.
43 N. M. Sammes, G. A. Tompsett, H. Nafe and F. Aldinger, *J. Eur. Ceram. Soc.*, 1999, **19**, 1801.
44 M. Morgensen, N. M. Sammes and G. A. Tompsett, *Solid State Ionics*, 2000, **129**, 63.
45 J. P. P Huijsmans, *Curr. Opin. Solid State Mater. Sci.*, 2000, **5**, 317.
46 L. Malavasi, C. A. J. Fisher and M. S. Islam, *Chem. Soc. Rev.*, 2010, **39**, 4370.
47 H. Mehrer, *Diffusion in Solids*, Springer, Berlin Heidelberg, 2007.
48 W. D. Kingery, H. K. Bowen, and D. R. Uhlmann, *Introduction to Ceramics*, Wiley, New York, 1976.
49 Y. M. Chiang, D. Birnie, and W. D. Kingery, *Physical Ceramics: Principles for Ceramic Science and Engineering*, MIT Press, Cambridge, 1997.

50 S. Miyoshi and M. Martin, *Phys. Chem. Chem. Phys.*, 2009, **11**, 3063.
51 P. R. Slater, J. T. S. Irvine, T. Ishihara and Y. Takita, *J. Solid State Chem.*, 1998, **139**, 135.
52 K. Laidler and C. King, *J. Phys. Chem.*, 1983, **87**, 2657.
53 R. Pornprasertsuk, P. Ramanarayanan, C. B. Musgrave and F. B. Prinz, *J. Appl. Phys.*, 2005, **98**, 103513.
54 M. Martin, *J. Electroceram.*, 2006, **17**, 765.
55 R. A. De Souza and M. Martin, *Monatsh. Chem.*, 2009, **140**, 1011.
56 E. A. Kotomin, Yu. A. Mastrikov, M. M. Kuklja, R. Merkle, A. Roytburd and J. Maier, *Solid State Ionics*, 2011, **188**, 1.
57 S. García-Martín, D. P. Fagg and J. T. S. Irvine, *Chem. Mater.*, 2008, **20**, 5933.
58 X. Xia, R. Oldman and R. Catlow, *Chem. Mater.*, 2009, **21**, 3576.
59 W. Smith and T. R. Forester, *J. Mol. Graphics*, 1996, **14**, 136.
60 J. D. Gale, *J. Chem. Soc., Faraday Trans.*, 1997, **93**, 629.
61 *Computer Modelling in Inorganic Crystallography*, ed. C. R. A. Catlow, Academic Press, San Diego, 1997.
62 M. D. Segall, P. J. D. Lindan, M. J. Probert, C. J. Pickard, P. J. Hasnip, S. J. Clark and M. C. Payne, *J. Phys.: Condens. Matter*, 2002, **14**, 2717.
63 P. Hohenberg and W. Kohn, *Phys. Rev.*, 1964, **136**, B864.
64 W. Kohn, *Rev. Mod. Phys.*, 1998, **71**, 1253.
65 W. Koch and M. C. Holthausen, *A Chemist's Guide to Density Functional Theory*, Wiley-VCH, Weinheim, 2001.
66 G. Henkelman, B. P. Uberuaga and H. Jónsson, *J. Chem. Phys.*, 2000, **113**, 9901.
67 M. Born and J. E. Mayer, *Z. Phys.*, 1932, **75**, 1.
68 R. A. Buckingham, *Proc. R. Soc. London, Ser. A*, 1938, **168**, 264.
69 R. W. Grimes, G. Busker, M. A. McCoy, A. Chroneos, J. A. Kilner and S. P. Chen, *Ber. Bunsen-Ges.*, 1997, **101**, 1204.
70 G. Busker, A. Chroneos, R. W. Grimes and I. W. Chen, *J. Am. Ceram. Soc.*, 1999, **82**, 1553.
71 Y. Takeda, R. Kanno, M. Noda and O. Yamamoto, *Bull. Inst. Chem. Res., Kyoto Univ.*, 1986, **64**, 157.
72 S. B. Adler, *Chem. Rev.*, 2004, **104**, 4791.
73 J. G. Bednorz and K. A. Müller, *Z. Phys. B: Condens. Matter*, 1986, **64**, 189.
74 S. J. Skinner, *Solid State Sci.*, 2003, **5**, 419.
75 E. J. Opila, H. L. Tuller, B. J. Wuensch and J. Maier, *J. Am. Ceram. Soc.*, 1993, **76**, 2363.
76 S. N. Savvin, G. N. Mazo and A. K. Ivanov-Schitz, *Crystallogr. Rep.*, 2008, **53**, 291.
77 J. L. Routbort, S. J. Rothman, B. K. Flandermeyer, L. J. Nowicki and J. E. Baker, *J. Mater. Res.*, 1988, **3**, 116.
78 J. A. Kilner and C. K. M. Shaw, *Solid State Ionics*, 2002, **154–155**, 523.
79 A. Chroneos, D. Parfitt, J. A. Kilner and R. W. Grimes, *J. Mater. Chem.*, 2010, **20**, 266.
80 D. Parfitt, A. Chroneos, J. A. Kilner and R. W. Grimes, *Phys. Chem. Chem. Phys.*, 2010, **12**, 6834.
81 A. Kushima, D. Parfitt, A. Chroneos, B. Yildiz, J. A. Kilner and R. W. Grimes, *Phys. Chem. Chem. Phys.*, 2011, **13**, 2242.
82 C. N. Munnings, S. J. Skinner, G. Amow, P. S. Whitfield and I. J. Davidson, *Solid State Ionics*, 2005, **176**, 1895.
83 M. Palcut, K. Wiik and T. Grande, *J. Phys. Chem. B*, 2007, **111**, 2299.
84 A. Maignan, C. Martin, D. Pelloquin, N. Nguyen and B. Raveau, *J. Solid State Chem.*, 1999, **142**, 247.
85 C. Zhu, X. Liu, C. Yi, D. Yan and W. Su, *J. Power Sources*, 2008, **185**, 193.
86 D. J. Chen, R. Ran and Z. P. Shao, *J. Power Sources*, 2010, **195**, 7187.
87 J. H. Kim, M. Cassidy, J. T. S. Irvine and J. Bae, *Chem. Mater.*, 2010, **22**, 883.
88 D. Parfitt, A. Chroneos, A. Tarancón and J. A. Kilner, *J. Mater. Chem.*, 2011, **21**, 2183.
89 J. Hermet, G. Geneste and G. Dezanneau, *Appl. Phys. Lett.*, 2010, **97**, 174102.
90 S. Streule, A. Podlensyak, D. Sheptyakov, E. Pomjakushina, M. Stingaciu, K. Conder, M. Medarde, M. V. Patrakeev, I. A. Leonidov, V. L. Kozhevnikov and J. Mesot, *Phys. Rev. B: Condens. Matter Mater. Phys.*, 2006, **73**, 94203.
91 A. Tarancón, D. Marrero-López, J. Peña-Martínez, J. C. Ruiz-Morales and P. Núñez, *Solid State Ionics*, 2008, **179**, 611.
92 J. Kilner, *Solid State Ionics*, 2000, **129**, 13.
93 A. A. Taskin, A. N. Lavrov and Y. Ando, *Prog. Solid State Chem.*, 2007, **35**, 481.
94 T. Norby, *J. Mater. Chem.*, 2001, **11**, 11.
95 A. Tarancón, A. Morata, G. Dezanneau and F. Peiró, *Fuel Cells*, 2011, **11**, 26.
96 H. B. Lee, F. B. Prinz and W. Cai, *Acta Mater.*, 2010, **58**, 2197.
97 C. A. J. Fisher and M. S. Islam, *Solid State Ionics*, 1999, **118**, 355.
98 T. Tsuchida and T. Kan, *J. Eur. Ceram. Soc.*, 2001, **21**, 555.
99 D. P. Fagg, V. V. Kharton, J. R. Frade and A. A. L. Ferreira, *Solid State Ionics*, 2003, **156**, 45.
100 M. V. Patrakeev, I. A. Leonidov, V. L. Kozhevnikov and V. V. Kharton, *Solid State Sci.*, 2004, **6**, 907.
101 N. Grunbaum, L. Mogni, F. Prado and A. Caneiro, *J. Solid State Chem.*, 2004, **177**, 2350.
102 J. A. Pardo, J. Santiso, C. Solís, G. Garcia, A. Figueras and M. D. Rossell, *Solid State Ionics*, 2006, **177**, 423.
103 L. Mogni, F. Prado and A. Caneiro, *Chem. Mater.*, 2006, **18**, 4163.
104 A. A. Markov, M. V. Patrakeev, V. V. Kharton, Y. V. Pivak, I. A. Leonidov and V. L. Kozhevnikov, *Chem. Mater.*, 2007, **19**, 3980.
105 A. Jones and M. S. Islam, *J. Phys. Chem. C*, 2008, **112**, 4455.
106 V. V. Kharton, E. V. Tsipis, V. A. Kolotygin, M. Avdeev, A. P. Viskup, J. C. Waerenborgh and J. R. Frade, *J. Electrochem. Soc.*, 2008, **155**, P13.
107 R. Bredesen, T. Norby, A. Bardal and V. Lynum, *Solid State Ionics*, 2000, **135**, 687.
108 M. V. Patrakeev, E. B. Mitberg, I. A. Leonidov and V. L. Kozhevnikov, *Solid State Ionics*, 2001, **139**, 325.
109 M. Y. Avdeev, M. V. Patrakeev, V. V. Kharton and J. R. Frade, *J. Solid State Electrochem.*, 2002, **6**, 217.
110 C. A. J. Fisher and M. S. Islam, *J. Mater. Chem.*, 2005, **15**, 3200.
111 S. Carter, A. Selcuk, R. J. Carter, J. Kajda, J. A. Kilner and B. C. H. Steele, *Solid State Ionics*, 1992, **53–56**, 597.
112 J. Sunstrom, K. V. Ramanujachary and M. Greenblatt, *J. Solid State Chem.*, 1998, **139**, 388.
113 E. V. Antipov, A. M. Abakumov and S. Y. Istomin, *Inorg. Chem.*, 2008, **47**, 8543.
114 S. Ya. Istomin, J. Grins, G. Svensson, O. A. Drozhzhin, V. L. Kozhevnikov, E. V. Antipov and J. P. Attfield, *Chem. Mater.*, 2003, **15**, 4012.
115 D. Rupasov, A. Chroneos, D. Parfitt, J. A. Kilner, R. W. Grimes, S. Ya. Istomin and E. V. Antipov, *Phys. Rev. B: Condens. Matter Mater. Phys.*, 2009, **79**, 172102.
116 D. Rupasov, et al., *Solid State Ionics*, in press.
117 M. Cherry, M. S. Islam and C. R. A. Catlow, *J. Solid State Chem.*, 1995, **118**, 125.
118 M. Yashima, K. Nomura, H. Kageyama, Y. Miyazaki, N. Chitose and K. Adachi, *Chem. Phys. Lett.*, 2003, **380**, 391.
119 M. S. Islam, *J. Mater. Chem.*, 2000, **10**, 1027.
120 O. H. Kwon and G. M. Choi, *Solid State Ionics*, 2006, **177**, 3057.
121 D. Pérez-Coll and G. C. Mather, *Solid State Ionics*, 2010, **181**, 20.
122 M. Feng and J. B. Goodenough, *J. Solid State Chem.*, 1994, **T31**, 663.
123 V. V. Kharton, F. M. B. Marques and A. Atkinson, *Solid State Ionics*, 2004, **174**, 135.
124 E. Bakken, N. L. Allan, T. Hugh, K. Barron, C. E. Mohn, I. T. Todorov and S. Stølen, *Phys. Chem. Chem. Phys.*, 2003, **5**, 2237.
125 C. E. Mohn, N. L. Allan, C. L. Freeman, P. Ravindran and S. Stølen, *J. Solid State Chem.*, 2005, **178**, 346.
126 S. A. Speakman, J. W. Richardson, B. J. Mitchell and S. T. Misture, *Solid State Ionics*, 2002, **149**, 247.
127 A. Nemudry, P. Weiss, I. Gainutdinov, V. Boldyrev and R. Schollhorn, *Chem. Mater.*, 1998, **10**, 2403.
128 R. Le Toquin, W. Paulus, A. Cousson, C. Prestipino and C. Lamberti, *J. Am. Chem. Soc.*, 2006, **128**, 13161.
129 W. Paulus, H. Schober, S. Eibl, M. Johnson, T. Berthier, O. Hernandez, M. Ceretti, M. Plazanet, K. Conder and C. Lamberti, *J. Am. Chem. Soc.*, 2008, **130**, 16080.
130 S. Inoue, M. Kawai, N. Ichikawa, H. Kageyama, W. Paulus and Y. Shimakawa, *Nat. Chem.*, 2010, **2**, 213.
131 N. Kitamura, K. Amezawa and Y. Tomii, *J. Electrochem. Soc.*, 2005, **152**, A658.
132 F. Schönberger, E. Kendrick, M. S. Islam and P. Slater, *Solid State Ionics*, 2005, **176**, 2951.

133 E. Kendrick, M. S. Islam and P. R. Slater, *J. Mater. Chem.*, 2007, **17**, 3104.

134 E. Kendrick, J. Kendrick, K. S. Knight, M. S. Islam and P. R. Slater, *Nat. Mater.*, 2007, **6**, 871.

135 S. Nakayama, T. Kageyama, H. Aono and Y. Sadaokac, *J. Mater. Chem.*, 1995, **5**, 1801.

136 S. Nakayama, H. Aono and Y. Sadaokac, *Chem. Lett.*, 1995, **6**, 431.

137 M. S. Islam, J. R. Tolchard and P. R. Slater, *Chem. Commun.*, 2003, 1486.

138 J. R. Tolchard, M. S. Islam and P. R. Slater, *J. Mater. Chem.*, 2003, **13**, 1956.

139 A. Jones, P. R. Slater and M. S. Islam, *Chem. Mater.*, 2008, **20**, 5055.

140 J. E. H. Sansom, D. Richings and P. R. Slater, *Solid State Ionics*, 2001, **139**, 205.

141 L. León-Reina, E. R. Losilla, M. Martínez-Lara, S. Bruque and M. A. G. Aranda, *J. Mater. Chem.*, 2004, **14**, 1142.

142 L. León-Reina, J. M. Porras-Vasquez, E. R. Losilla and M. A. G. Aranda, *J. Solid State Chem.*, 2007, **180**, 1250.

143 J. E. H. Sansom, J. R. Tolchard, D. Apperley, M. S. Islam and P. R. Slater, *J. Mater. Chem.*, 2006, **16**, 1410.

144 J. Maier, *Nat. Mater.*, 2005, **4**, 805.

145 M. G. Blamire, J. L. MacManus-Driscoll, N. D. Mathur and Z. H. Barber, *Adv. Mater.*, 2009, **21**, 3827.

146 M. Mavrikakis, B. Hammer and J. K. Norskov, *Phys. Rev. Lett.*, 1998, **81**, 2819.

147 J. A. Kilner, *Nat. Mater.*, 2008, **7**, 838.

148 S. J. Litzelman, J. L. Hertz, W. Jung and H. L. Tuller, *Fuel Cells*, 2008, **8**, 294.

149 A. Kushima, S. Yip and B. Yildiz, *Phys. Rev. B: Condens. Matter Mater. Phys.*, 2010, **82**, 115435.

150 N. Schichtel, C. Korte, D. Hesse and J. Janek, *Phys. Chem. Chem. Phys.*, 2009, **11**, 3043.

This journal is © The Royal Society of Chemistry 2011

Energy Environ. Sci., 2011, **4**, 2774–2789 | 2789